Received: 20 October 2016 | Accepted: 24 October 2016

DOI: 10.1111/ijac.12623

ORIGINAL ARTICLE

International Journal of Applied Ceramic TECHNOLOGY

In situ synthesis of Al_2O_3-supported $ZnCr_2O_4$ nanoparticles for application as an activated photocatalyst

Hamid Tajizadegan[1] | Sanaz Naghibi[2,3] | Amin Jamshidi[1] | Omid Torabi[1] | Mohammad-Hossein Golabgir[1]

[1]Young Researchers and Elite Club, Najafabad Branch, Islamic Azad University, Najafabad, Iran

[2]Department of Materials Engineering, Shahreza Branch, Islamic Azad University, Shahreza, Iran

[3]Razi Chemistry Research Center (RCRC), Shahreza Branch, Islamic Azad University, Shahreza, Iran

Correspondence
H. Tajizadegan,
Email: hamid_tjz@yahoo.com

Abstract

Zincochromite nanoparticles (NPs) were precipitated on surfaces of the as-prepared Al_2O_3 micron-sized particles by a heterogeneous precipitation technique using urea as a homogeneous precipitation agent. This procedure leads to decrease the pore diameter and increase the pore volume and specific surface area (a_s), realizing the potential access to $ZnCr_2O_4$ catalytic sites. Although the obtained band gap energy (E_g) of Al_2O_3-$ZnCr_2O_4$ composite is about 2.3 eV (more than $ZnCr_2O_4$), the absorbance is enhanced about 1.5 orders of magnitude. These characteristics make it an effective photocatalyst of inorganic dyes from an aqueous media. Dye removal performance of the nanocomposite powder is higher than that of pure $ZnCr_2O_4$, which is attributed to an increase in the photocatalytic sites and the absorbance intensity. It was believed that the surface area created from Al_2O_3 support realized the potential access to $ZnCr_2O_4$ catalytic sites. To confirm these assertions, X-ray diffractometry (XRD), scanning electron microscopy (SEM), diffuse reflectance spectroscopy (DRS), and N_2 adsorption-desorption analysis were applied.

KEYWORDS

chemical synthesis, composites, diffuse reflectance spectra, X-ray diffraction, zincochromite

1 | INTRODUCTION

The spinel compounds are any materials composed of divalent and trivalent ions with general formulation of AB_2X_4, where A, B, and X are divalent cation, trivalent cation and anion, respectively.[1] The oxide spinels are widely known and find some applications such as the following:

- Magnesium aluminates ($MgAl_2O_4$) is used for optically transparent ceramic usages, neutron radiation resistance applications, humidity sensors, refractories, catalyst, and catalyst supports.[2]
- Gahnite ($ZnAl_2O_4$) as a catalyst is applied to degrade the gaseous toluene,[3] reform the ethanol steam,[4] and complete treatment of NO_x.[5]
- Magnetite (Fe_3O_4) is employed for biomedical applications,[6,7] water treatments[8,9] and magnetic adsorbent.[10]
- Zincochromite ($ZnCr_2O_4$) is one of the chromium spinels with the humidity sensing performance,[11] photocatalytic behavior,[12] and magnetic properties.[13,14]

Various methods have been applied to synthesize $ZnCr_2O_4$ and its composites, including mechanical mixing and heat treatment of ZnO-Cr_2O_3 powder mixtures,[15] direct calcinations of ZnO-Cr_2O_3 powder mixture,[16] thermal decomposition of Zn-Cr gel achieved from sol gel technique,[17] thin film fabrication by RF sputtering system,[18] etc. Since the photocatalytic and catalytic behaviors of the synthesized $ZnCr_2O_4$ are important factors determining its applications, the researchers focus on the special methods enhancing these properties by decreasing the particle size and/or increasing the a_s.[19-21] It is very important to choose the best preparation method and materials to obtain a pure

and highly active product with high a_s. One of the leading studies is by Peng et al. They have been used a simple hydrothermal route to synthesize $ZnCr_2O_4$ NPs with average particle size of 5 nm and direct band gap about 3.46 eV.[12] Gingasu et al. have been synthesized $ZnCr_2O_4$ NPs using precursor method via thermal decomposition of tartarate compound and gluconate compound. The average crystallite size and a_s are approximately 60 nm and 77 m^2/g.[22] Mousavi et al. have been recently reported a facile co-precipitation method to achieve $ZnCr_2O_4$ NPs from $Zn(NO_3)_2{\cdot}6H_2O$ and $CrCl_3{\cdot}6H_2O$. The average particle size was measured as ~70 nm with remarkable activity for dye removing from waste water.[23] As described elsewhere,[24] $ZnCr_2O_4$ NPs (with the average particle size of 13 nm) have been prepared by a simple and cheap homogeneous precipitation method using urea hydrolysis followed by heat treatment at 500°C. The a_s has been reported to be about 47 m^2/g. Although some improvements have been obtained by the mentioned methods, this research is focused on increasing the a_s by applying Al_2O_3 as the crystallization sites.

The aim of this research is to enhance the procedure used in the previous work[24] by applying Al-containing precursor to act as the precipitation site. It is expected that the existence of Al_2O_3 nuclei will diminish the agglomeration of the as-synthesized NPs and exhibit a remarkable improvement over the a_s.

2 | EXPERIMENTAL

2.1 | Raw chemicals and preparation method

The $ZnCr_2O_4$ NPs were synthesized as described elsewhere,[24] using zinc acetate dehydrate [$Zn(CH_3COO)_2{\cdot}2H_2O$ (Merck, Hohenbrunn, Germany)] as a zinc source, chromium nitrate [$Cr(NO_3)_2{\cdot}9H_2O$ (Merck)] as a chromium source, and urea powder [NH_2CONH_2 (Merck)] as a hydrolyzing agent. To prepare Al_2O_3-$ZnCr_2O_4$ nanocomposite, a simple method has been applied which was previously reported to synthesize Al_2O_3-ZnO nanocomposite. Aluminum hydroxide powder [$Al(OH)_3$ (Bayerite-type, Ardakan Industrial Ceramics Co., Ardakan, Iran)] was used as an Al-containing precursor to provide Al_2O_3 seeds in the precipitation media.[25,26]

At the first step, zinc acetate dehydrate and chromium nitrate were mixed with the molar ratio of 1:2 to obtain a 0.3 mol/L solution, and then a large amount of urea was added to the solution under string to adjust the molar ratio of urea: [Zn^{2+}+Cr^{3+}] to 6:1. In order to provide Al ions, an adequate amount of aluminum hydroxide solution [$Al(OH)_3$ (3 μm, Bayerite-type, Ardakan Industrial Ceramics Co., Iran)] was added into the suspension during stirring. The solution was continuously stirred at 25°C for 2 h, sonicated for 20 min and then refluxed in an oil bath at 90°C for 24 h.

The pH change is an index of urea hydrolysis. The pH initial value, ie, before the addition of urea, was about 6. It did not increase significantly by adding urea due to its thermal stability. The reflux process provides sufficient energy for urea decomposition and gradual increase in pH, reaching necessary value for metal hydroxides precipitation. The progression of precipitation leads to decrease in metal precursor and consequently increase in pH. The pH value of the experimented solution reached to ~9 at the end of the reflux period.[27,28]

This procedure provides the conditions under which urea hydrolysis occurs and consequently the metal ions-containing compounds precipitate.[29] It is expected that the mentioned method would lead to form $Zn^{2+}/Cr^{3+}/Al^{3+}$-containing precipitate, based on the heterogeneous precipitation theory.[30]

After filtering and washing with distilled water, the obtained precipitate was dried at 160°C overnight, and then calcined at 500°C for 3 h. (The calcinations temperature was chosen based on the simultaneous thermal analysis (STA) results representing in Section 3.)

For a comparative purpose, pure $ZnCr_2O_4$ and Al_2O_3 were also prepared. High-purity Al_2O_3 powder and also $ZnCr_2O_4$ powder were prepared by co-precipitation method through urea hydrolysis through the same procedure, as mentioned for $ZnCr_2O_4$-Al_2O_3.

2.2 | Characterization

The phase identification was carried out by powder X-ray diffraction (XRD, Philips, Eindhoven, Netherland). The thermal behaviors of the as-prepared samples were perused with differential thermal and thermo-gravimetric analysis (DTA and TG), using a thermal analyzer (METTLER TGA/SDTA 851E, Mettler-Toledo Ltd., Leicester, UK) at a heating rate of 10°C/min from room temperature to 1000°C. The morphology and particle size of the product were studied by field-emission scanning electron microscopy (FE-SEM, Hitachi S-4160, Tokyo, Japan), and also chemical microanalyses of the samples were identified by energy dispersive spectroscopy (EDS-MAP). The diffuse reflectance spectra (DRS) were collected by a spectrophotometer (V-670, Jasco, Easton, PA). The Tauc method was applied to determine the optical band gap energy (E_g) via plotting $(\alpha h\upsilon)^2$ against hυ, where α is the absorption coefficient and hυ is the photon energy and then the linear part of the curve extrapolated to $(\alpha h\upsilon)^2=0$.[31]

To specify the specific surface area and pore characteristics, the N_2 adsorption-desorption analysis was performed at 77 K by a surface area analyzer (Micromeritics ASAP-2010, Norcross, GA), and the required results were obtained by applying the Brunauer-Emmett-Teller (BET), Barrett-Joyner-Halenda (BJH), and Dollimore-Heal (DH)

methods. The volume of N_2 adsorbed at the completion of a monolayer at IUPAC established standard temperature and pressure (V_m), energy constant in the first layer (C), *mean pore diameter*, total specific surface area (a_s), and *total pore volume* (at p/p_0=0.990) were calculated based on the BET model. The pore volume (V_p), pore distribution peak ($r_{p\ peak}$) and pore specific surface area (a_p) were determined using BJH and DH techniques.

The dye removal performance as an index of the photocatalytic activity was evaluated for the as-synthesized $ZnCr_2O_4$ and Al_2O_3-$ZnCr_2O_4$ samples by investigating the decomposition behavior of methylene blue (MB) irradiated with 365 nm ultra-violet lamp (2×15 W, Philips). TiO_2-P25 (AEROXIDE, Degussa, Evonik, Essen, Germany) as a standard commercial photocatalyst was used for comparing the results. For this purpose, an aqueous MB solution (30 mg/L) was prepared and then 50 mg of each powder ($ZnCr_2O_4$, Al_2O_3-$ZnCr_2O_4$, and TiO_2-P25) was added to the 50 mL of MB solution. The UV irradiation was performed for 2 h at room temperature with the distance of 10 cm. Then, the solutions were centrifuged and NPs were separated from the solution. The MB concentrations were measured by a UV-visible spectrophotometer at 664 nm.

3 | RESULTS AND DISCUSSION

As described in a previous paper, $ZnCr_2O_4$ was successfully prepared by the homogeneous precipitation method[24]; therefore, its characteristics would be considered as a comparison index to evaluate the influences of the Al_2O_3 particles on the phase component, optical properties, and the specific surface area of the obtained compound.

Thermal analysis helps to determine the required heat treatment schedule. Figure 1 shows the TGA and DTA curves of the as-prepared Zn/Cr and Al/Zn/Cr containing powders. As can be seen, the thermal behaviors of both samples are similar and the temperature region in which the unique exothermic reaction occurred is 300-500°C. This event accompanied with the mass loss can be associated with a chemical conversion. However, commenting on this subject needs more characterizations. What can be inferred from this figure is the heat treatment schedule that was chosen as 500°C for 3 h. This condition can guarantee the completion of the mentioned chemical reaction.

Figure 2(a-c) shows the XRD results of the calcined samples; the Al containing powder, the Zn/Cr containing powder and the Al/Zn/Cr containing sample. In the first pattern, a low crystalline powder containing a trace of γ-Al_2O_3 [JCPDF # 1-1308] has been observed. A mixture of $Al(OH)_3$ and urea was dried and calcined at 500°C and a semi-crystalline γ-Al_2O_3 powder was achieved. The low intensity and wide peaks confirm that this calcination temperature is not adequate for complete crystallization of Al_2O_3. However, these particles could be synthesized via this process. The second pattern is related to the Zn/Cr containing powder. As it was explained elsewhere, $ZnCr_2O_4$ NPs could be achieved via homogeneous

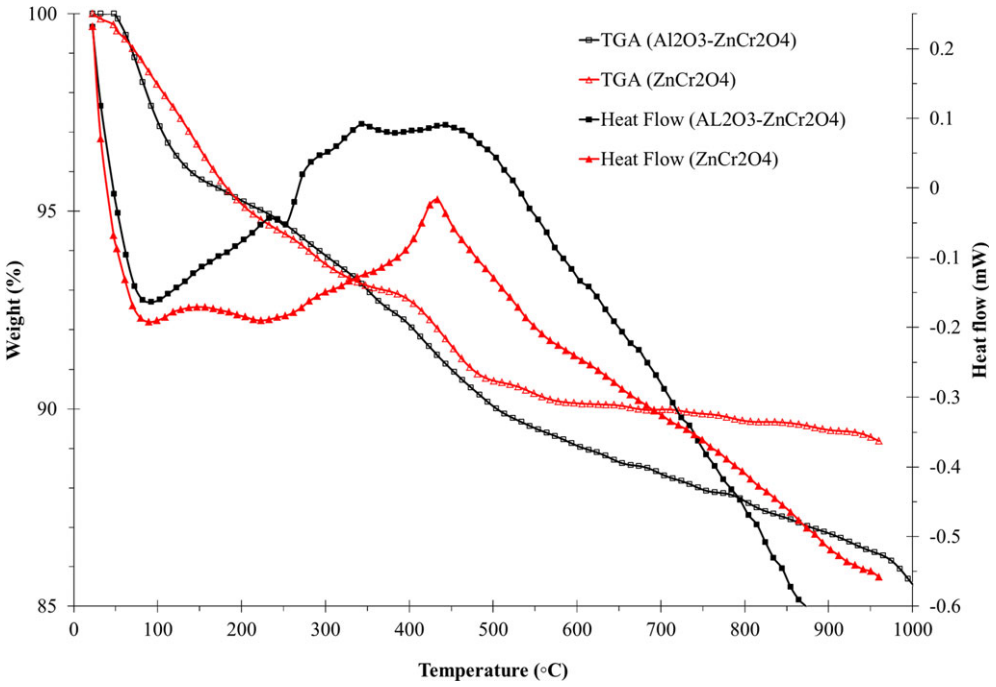

FIGURE 1 TGA and DTA curves of the as-prepared Zn/Cr and Al/Zn/Cr containing powders. [Color figure can be viewed at wileyonlinelibrary.com]

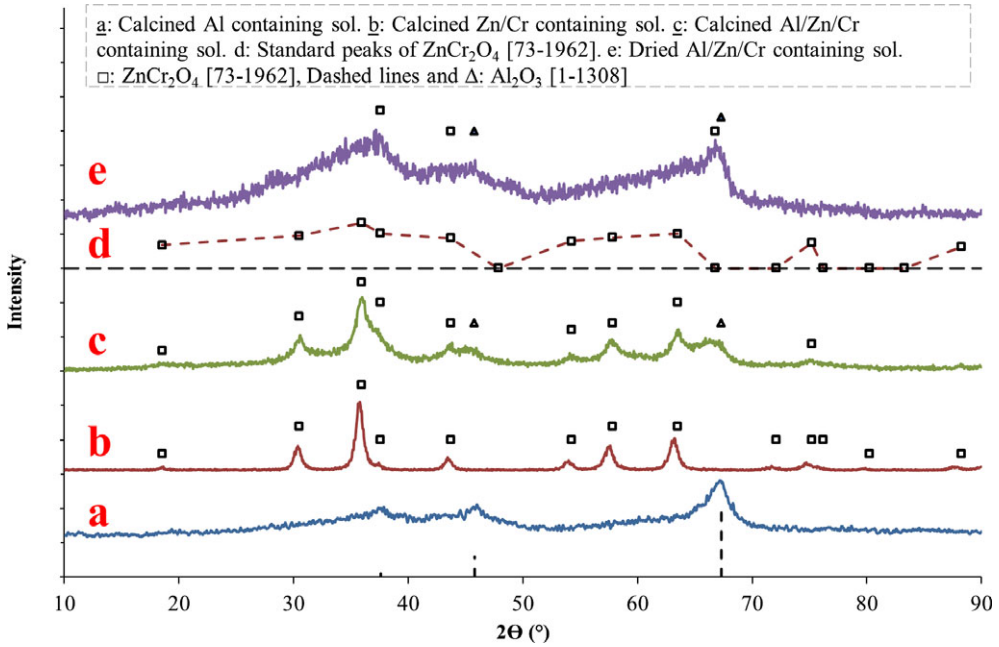

FIGURE 2 XRD results of the experimented powders. (a): Calcined Al containing sol. (b): Calcined Zn/Cr containing sol. (c): Calcined Al/Zn/Cr containing sol. (d): Standard peaks of $ZnCr_2O_4$ [JCPDF # 73-1962]. (e): Dried Al/Zn/Cr containing sol. [Color figure can be viewed at wileyonlinelibrary.com]

precipitation method from Zn/Cr containing solution.[24] The third pattern is related to the aim of this manuscript namely the Al/Zn/Cr containing solution. It is clear that the XRD pattern of this sample is the sum of the previous two patterns. All the intense peaks are corresponding to $ZnCr_2O_4$ [JCPDF # 73-1962], whereas the basic shape of this pattern is similar to that of the Al-containing sample. It means that a ceramic/ceramic composite powder consisting of Al_2O_3/$ZnCr_2O_4$ has been synthesized.

The sequence of phase formation before and after the calcination process has been evaluated utilizing XRD. Figure 2(c,e) shows the results, illustrating that the dried sample consists mainly of Al_2O_3, whereas the phase components change during calcination in which $ZnCr_2O_4$ is synthesized. It can be concluded that the nuclei and/or crystallites of Al_2O_3 could be synthesized during drying; therefore, its related peaks are tiny and wide. In other word, feature of the dried powder (Figure 2e) is similar to the standard peaks of $ZnCr_2O_4$ [JCPDF # 73-1962] (Figure 2d), as well as traces of Al_2O_3 characteristic peaks (triangles at about 46° and 67°). The Al_2O_3 crystallites could act as nucleation sites that could facilitate the nucleation of $ZnCr_2O_4$ phase. Due to multiplicity of sites where the $ZnCr_2O_4$ nuclei can be crystallized, the heterogeneous precipitation can be accepted for this preparation method. This claim would be explained in the following paragraphs.

FESEM-EDS elemental mapping of the as-synthesized Al_2O_3-$ZnCr_2O_4$ composite powder reveals the $ZnCr_2O_4$ particles distribution over the Al_2O_3 support. As can be seen in Figure 3, Al and O have been distributed over the map with higher concentration; mine while, Cr and Zn have distributed uniformly with low concentrations. These results consolidate the hypothesis that $ZnCr_2O_4$ NPs precipitate over Al_2O_3 particles, improving their characteristics. Base on this analysis, the O, Al, Cr, and Zn atomic percentage (at. %) were estimated about 53, 20, 14, and 6, respectively. Therefore, the mole ratio of $ZnO:Cr_2O_3:Al_2O_3$ in the as-synthesized powder was calculated about 6:7:10. Similarly, the mole ratio of $ZnCr_2O_4/Al_2O_3$ was estimated about 6.5/10 and the mole percentage of $ZnCr_2O_4$ in the composite powder was achieved about 40%.

The morphology of the as-synthesized compound is the main factor distinguishing its physical properties. Figure 4 shows the FE-SEM images of the dried precipitate (Figure 4A,B) and the calcined powder (Figure 4C,D) of Al_2O_3- $ZnCr_2O_4$. The porous structure of the $ZnCr_2O_4$ powder is also provided in Figure 4E (This figure has been originally published in the previous work[24]). There are some micron particles in the dried precipitate powder (see Figure 4A) which was originated from $Al(OH)_3$ powder. These particles are probably the mentioned sites for new phase nucleation. Figure 4B shows the surface of this particle with higher magnification. As can be seen, precipitates particles with less than 10 nm size and similar shapes were formed. Although micron size particles retain after calcinating the powder (see Figure 4C), the morphology and size of the nano-size particles on the surface of the micron-size particles had been changed. The heat treatment led to the removal of the inorganic part of the particles, by rising up

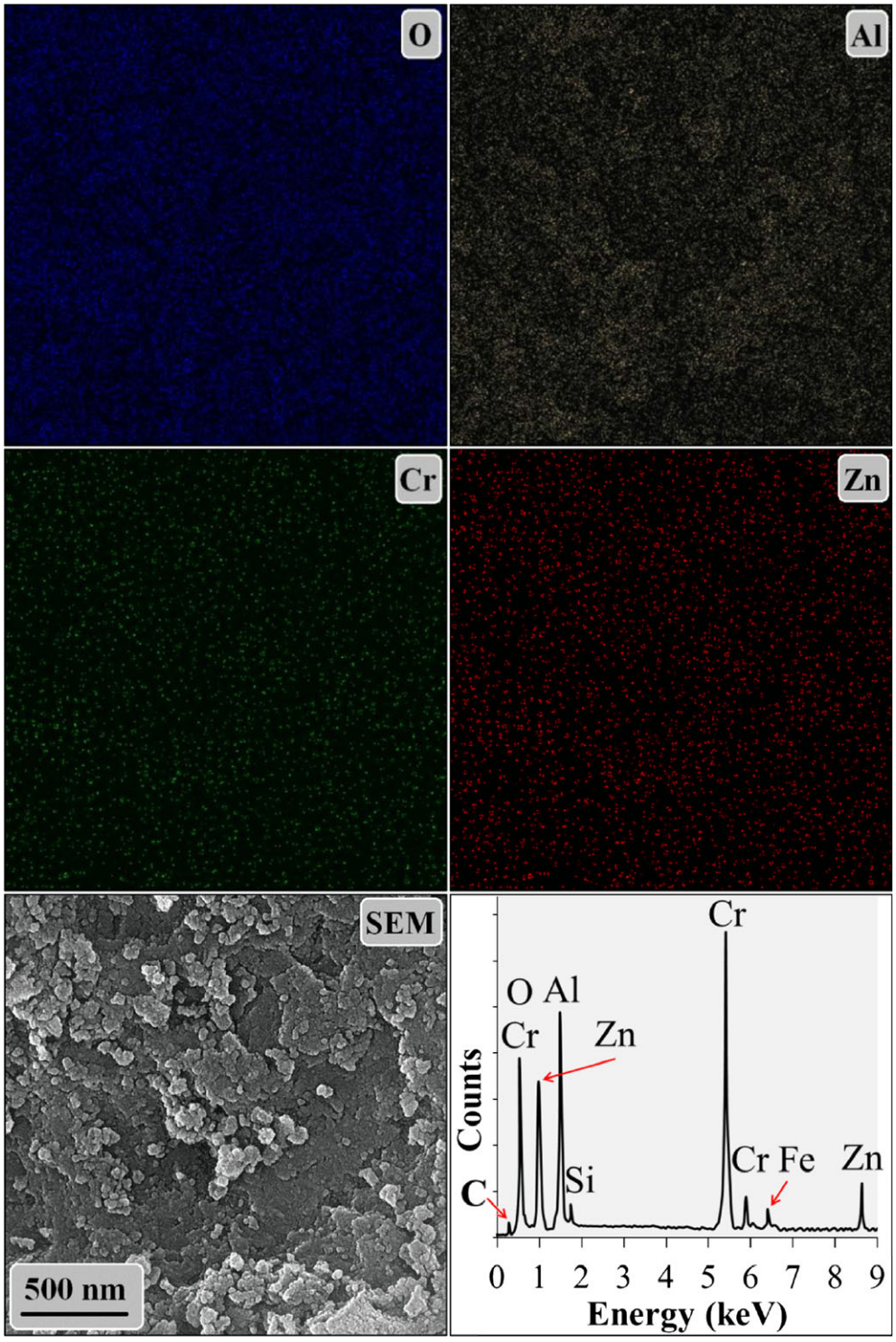

FIGURE 3 Elemental distribution map of the as-synthesized powder. [Color figure can be viewed at wileyonlinelibrary.com]

of a gaseous compound. On the other hand, the tendency of NPs to agglomerate could lead to particles representing irregular agglomeration with a wide range of size distribution. These two phenomena are the main reasons for differences between Figure 4B,D. However, the observation of the as-synthesized NPs on the surface of the micron-size particles is a remarkable result, regardless of the size and morphology. Figure 4E shows the FESEM image of the $ZnCr_2O_4$ particles without any seed as the nucleation site.[24] This figure confirms that the microstructure of the $ZnCr_2O_4$ NPs is a porous one and that the particles are joined to each other, hence forming welded agglomerates. The differences between Figure 4D,E are ascribed to the existence of Al-compound in the solution. For this reason,

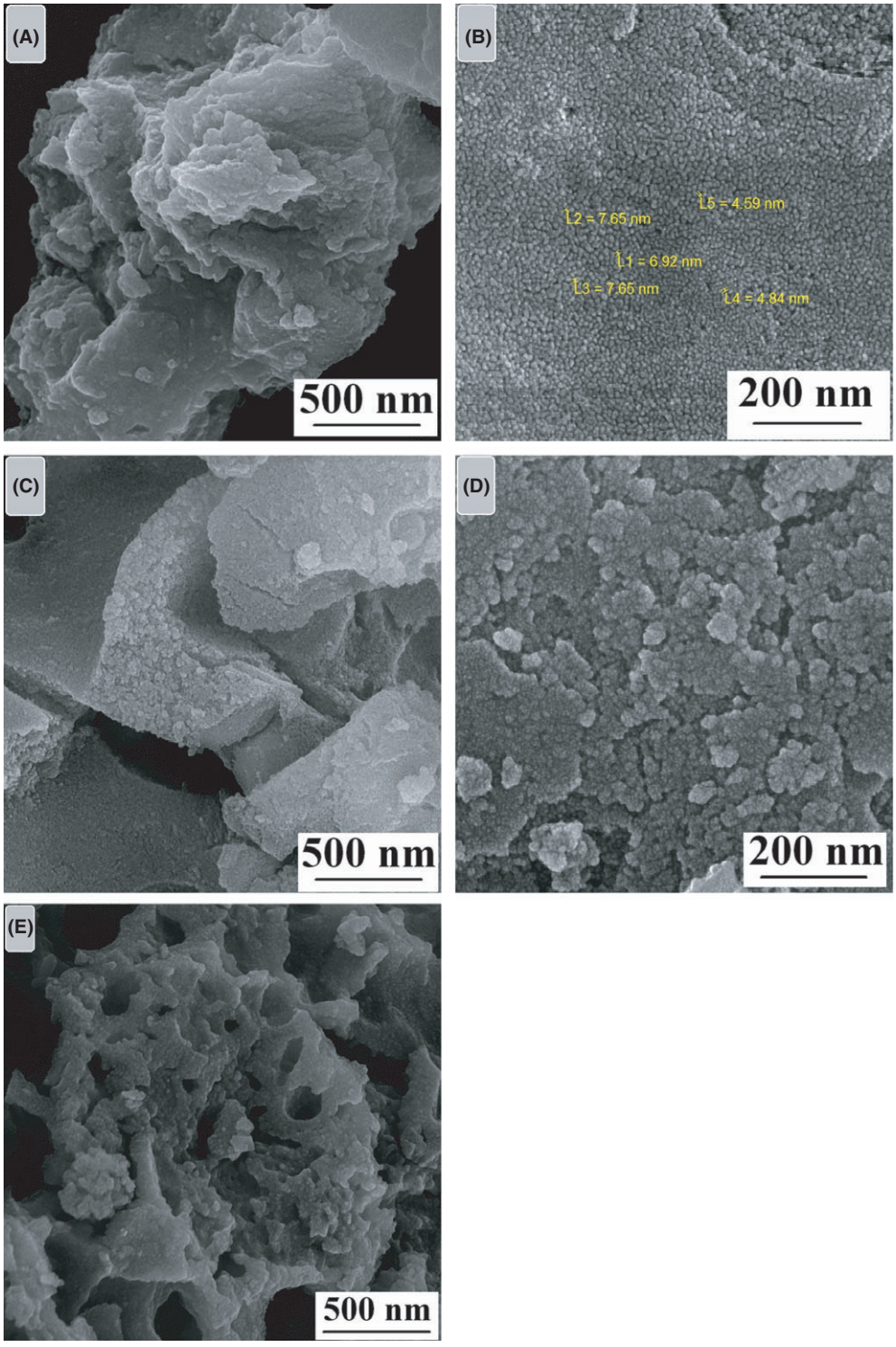

FIGURE 4 FESEM images of the dried precipitate (A and B), the calcined Al_2O_3- $ZnCr_2O_4$ composite powder (C and D), and the porous structure of the $ZnCr_2O_4$ powder (This figure has been originally published in the previous work[24]). [Color figure can be viewed at wileyonlinelibrary.com]

Al-containing particles act as the nucleation sites and $ZnCr_2O_4$ NPs could crystallize on the surface of the as-formed Al_2O_3 particles.

The conversion of $Al(OH)_3$ to Al_2O_3 and formation of the Al_2O_3- $ZnCr_2O_4$ composite powder with the mentioned microstructure could improve some of the characteristics owned by the as-synthesized $ZnCr_2O_4$ powder. One of the most important parameters influencing the photo catalytic activity is the specific surface area[32] that would be certainly influenced by the particles morphology. Figure 5 shows the nitrogen adsorption—desorption isotherm, BET, BJH, and DH plots. The calculated values of V_p, a_p, $r_{p\ peak}$,

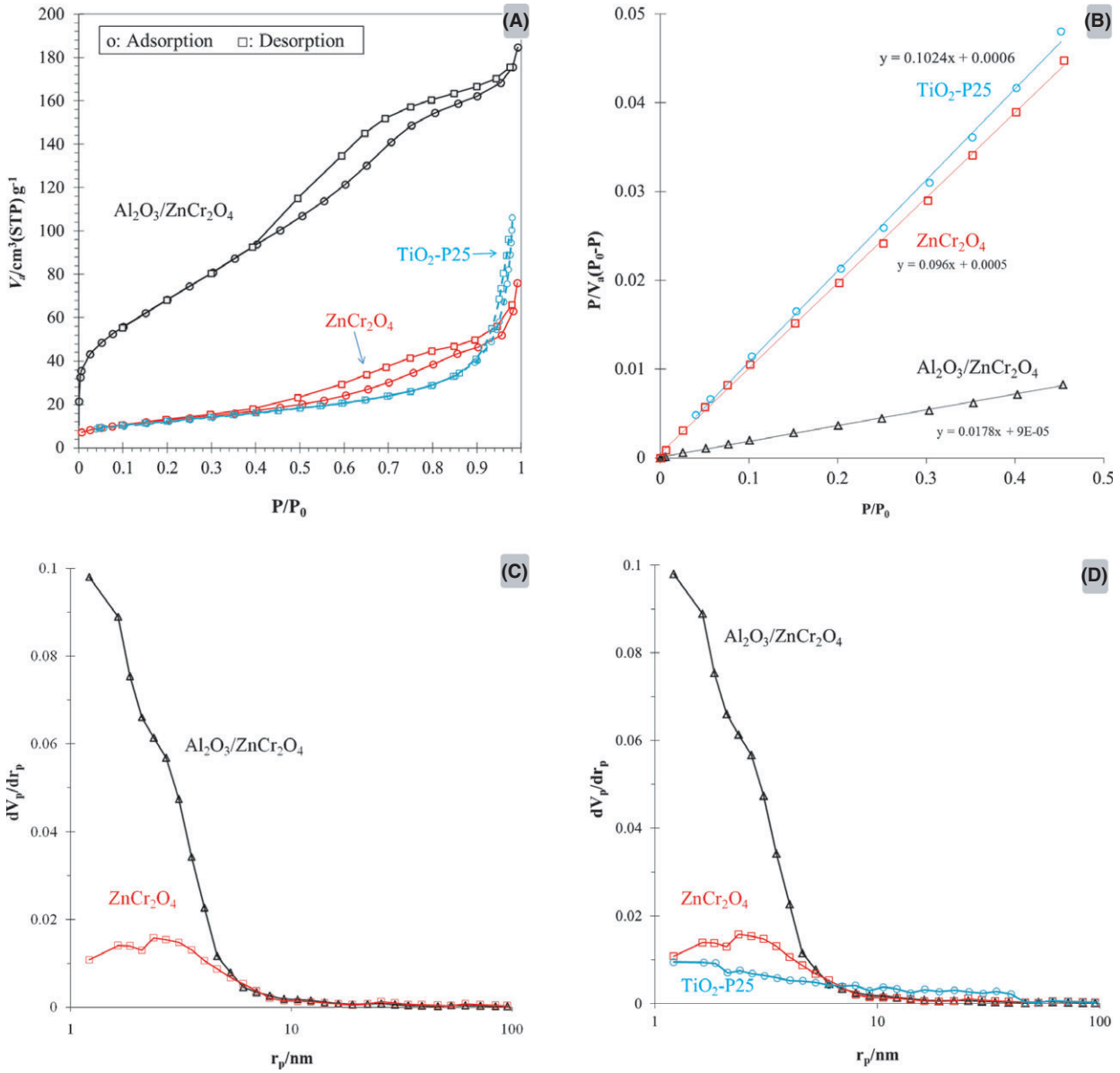

FIGURE 5 (A) The N_2 adsorption-desorption isotherm, (B) the BET, (C) the BJH and (D) the DH plots of the as-synthesized Al_2O_3- $ZnCr_2O_4$, $ZnCr_2O_4$, and TiO_2-P25 powders. [Color figure can be viewed at wileyonlinelibrary.com]

V_m, *C*, *mean pore diameter*, a_s, and *total pore volume* are provided in Table 1.

Figure 5A shows the physical adsorption-desorption isotherm of the Al_2O_3- $ZnCr_2O_4$, $ZnCr_2O_4$, and TiO_2-P25 samples. It is clear that the feature of the as-synthesized Al_2O_3- $ZnCr_2O_4$ composite is similar to type IV in the IUPAC classification features, whereas the shapes of the $ZnCr_2O_4$ and TiO_2-P25 samples are more similar to type V and III, respectively. This means that the interaction between the particles surface and N_2 is stronger in the composite powder in comparison to the bare $ZnCr_2O_4$ and TiO_2-P25 samples. Although the types of the isotherm plots are not similar, both of the samples (Al_2O_3-$ZnCr_2O_4$ and $ZnCr_2O_4$) can be considered as mesoporous materials. The calculated *mean pore diameters* of the Al_2O_3- $ZnCr_2O_4$, $ZnCr_2O_4$, and TiO_2-P25 samples are about 4.5, 10, and 15 nm, respectively, supporting this assumption.

According to Figure 5B, the slope of the BET line of the composite powder is less than that of the bare and TiO_2-P25 samples. The calculated values confirmed that the specific surface area of the composite powder was ~250 m^2/g, which is approximately five times greater than those of the bare $ZnCr_2O_4$ and TiO_2-P25 samples (a_s=47 and 43 m^2/g, respectively). The *mean pore size* and *total pore volume* of the composite sample were ~4.5 nm and ~0.28 cm^3/g, about two times smaller and two times greater than those of the $ZnCr_2O_4$ sample, respectively. The BET results showed that using $Al(OH)_3$ in the preparation process led to form a powder with higher surface area and pore volume and smaller

TABLE 1 The values of specific surface area and pore characteristics of the as-synthesized Al_2O_3- $ZnCr_2O_4$, $ZnCr_2O_4$, and TiO_2-P25 powders

Parameter [unit]	Source	Al_2O_3- $ZnCr_2O_4$	$ZnCr_2O_4$	TiO_2-P25
V_m [cm^3(STP)/g]	BET	58.56	10.73	9.88
C	BET	58	78	106
Mean pore diameter [nm]	BET	4.45	9.85	15.24
a_s [m^2/g]	BET	255	47	43
Total pore volume [cm^3/g]	BET	0.2835	0.1150	0.1639
V_p [cm^3/g]	BJH	0.2643	0.1144	0.1362
a_p [m^2/g]	BJH	232	51	40
$r_{p\ peak}$ (area) [nm]	BJH	1.21	2.38	1.22
V_p [cm^3/g]	DH	0.2878	0.1223	–
a_p [m^2/g]	DH	277	67	–
$r_{p,peak}$ (area) [nm]	DH	1.64	1.64	–

pores size; therefore, a large number of small pores are distributed throughout the sample. The SEM images confirm this finding (see Figure 4D,E). According to Table 1, V_m (adsorbed-N_2 volume) values show a sharp elevation by applying $ZnCr_2O_4$ on Al_2O_3 particles. This can be related to the formation of high textural porosity by distributing of the as-synthesized $ZnCr_2O_4$ on the Al_2O_3 surface and generating interparticle spaces. This event affects the pore volume. The *total pore volume* and V_p values of the Al_2O_3- $ZnCr_2O_4$ sample are two times greater than those of $ZnCr_2O_4$ powder. The other important parameter determining the specific surface area (a_s) is the pore size. This parameter is determined as *mean pore diameter* and $r_{p,peak}$. The average pore diameter of Al_2O_3- $ZnCr_2O_4$ is less than that of $ZnCr_2O_4$. This was achieved from BET, BJH, and DH results. The reason has been explained before. These two matters (increase in the pore volume and decrease in the pore size) lead to increase the specific surface area, which is very important in enhancing the photocatalytic behaviors.

In other words, the textural characteristics of the Al_2O_3-$ZnCr_2O_4$ nanocomposite powder are superior to $ZnCr_2O_4$ NPs, due to more surface positions for crystallization, dispersing and growth of $ZnCr_2O_4$ NPs, and as a consequence the agglomeration would be restricted. Thus, it is predicted that higher surface area accelerates the accessibility of reactant molecules to the catalytic sites of $ZnCr_2O_4$. The BJH and DH results support the BET and SEM observations.

The optical absorption spectra (UV-DRS) of the samples are illustrated in Figure 6A. Estimation of the E_g values based on the Tauc method is provided in Figure 6B. As can be observed, the $ZnCr_2O_4$ sample absorbed the light at 250-600 nm wavelength regions with low intensity, whereas the as-synthesized composite powder is characterized by a high absorbance at 250-500 nm. This means that although the preparation of $ZnCr_2O_4$ on the surface of Al_2O_3 particles led to intensify the absorption peaks, the absorption region is restricted to a narrower wavelength region. In the case of TiO_2-P25, only the subtractive absorption in the region of wavelength more than 400 nm is detected and the area under curve of this powder is very fewer than those of the as-synthesized $ZnCr_2O_4$ and Al_2O_3-$ZnCr_2O_4$.

Since Cr ion contains unpaired electrons in d orbital, the d-d transition of Cr-containing materials determines their behavior under UV-visible illumination. The Cr-d3 coordination in $ZnCr_2O_4$ and Al_2O_3-$ZnCr_2O_4$ powder are not similar. In the case of $ZnCr_2O_4$, there are three small bands at around 250, 330, and 580 nm, corresponding to an octahedral environment. The bands characteristics of this coordination are as below: $^4A_{2g}\rightarrow{}^4T_{1g}$ (P) in 200-300 nm, $^4A_{2g}\rightarrow{}^4T_{1g}$ (F) in <450 nm, and $^4A_{2g}\rightarrow{}^4T_{2g}$ in <580 nm.[22] This is in good agreement with the obtained results.

The other part of this figure is related to Al_2O_3-$ZnCr_2O_4$ powder. As can be seen, there are two relatively intense bands at around 255 and 360 nm, and also one small band at 580 nm. The latter is assigned to the transition of $^4A_{2g}$ to $^4T_{2g}$ and not important due to its low intensity. The other peaks are similar to those of $ZnCr_2O_4$ powder and assigned to the transition of $^4A_{2g}$ to $^4T_{1g}$. The first peak at around 255 nm can be related to band gap absorption of Al_2O_3-$ZnCr_2O_4$ powder. For this reason, the E_g values were about 1.8 and 2.3 eV for the $ZnCr_2O_4$ and Al_2O_3-$ZnCr_2O_4$ samples, respectively. Considering that the E_g value of Al_2O_3 is about 8.8 eV, the difference between E_g values of Al_2O_3 and the as-synthesized $ZnCr_2O_4$ is 7 eV, creating a band offset for the as-synthesized Al_2O_3-$ZnCr_2O_4$ in the range of 1.8-8.8 eV. The obtained results show that this value is about 2.3 eV. Although this phenomenon has been reported for Al_2O_3- ZnO[33] and Al_2O_3-SnO[34] systems, this is the first demonstration for the $ZnCr_2O_4$ NPs.

Figure 7 shows the influences of the as-prepared samples and TiO_2-P25 on the degradation of MB after 2 h of UV irradiation. As can be seen, 2 h of irradiation to MB suspension led to decrease its concentration about 20%. Considering the black line (2 h irradiated MB suspension) as an indicator of comparison, it is clear that the $ZnCr_2O_4$, TiO_2-P25, and Al_2O_3- $ZnCr_2O_4$ samples caused ~14%, 40% and 86% MB degradation, respectively. This phenomenon might be related to the photocatalytic performance of the powder samples, confirming the higher efficiency of the as-synthesized Al_2O_3-$ZnCr_2O_4$ sample in comparison with the pristine $ZnCr_2O_4$ or TiO_2-P25 NPs.

These promising achievements maybe related to the increase of the active sites of modified $ZnCr_2O_4$ NPs by depositing on Al_2O_3 particles. Actually, this improvement occurs with the increase in the specific surface area of the

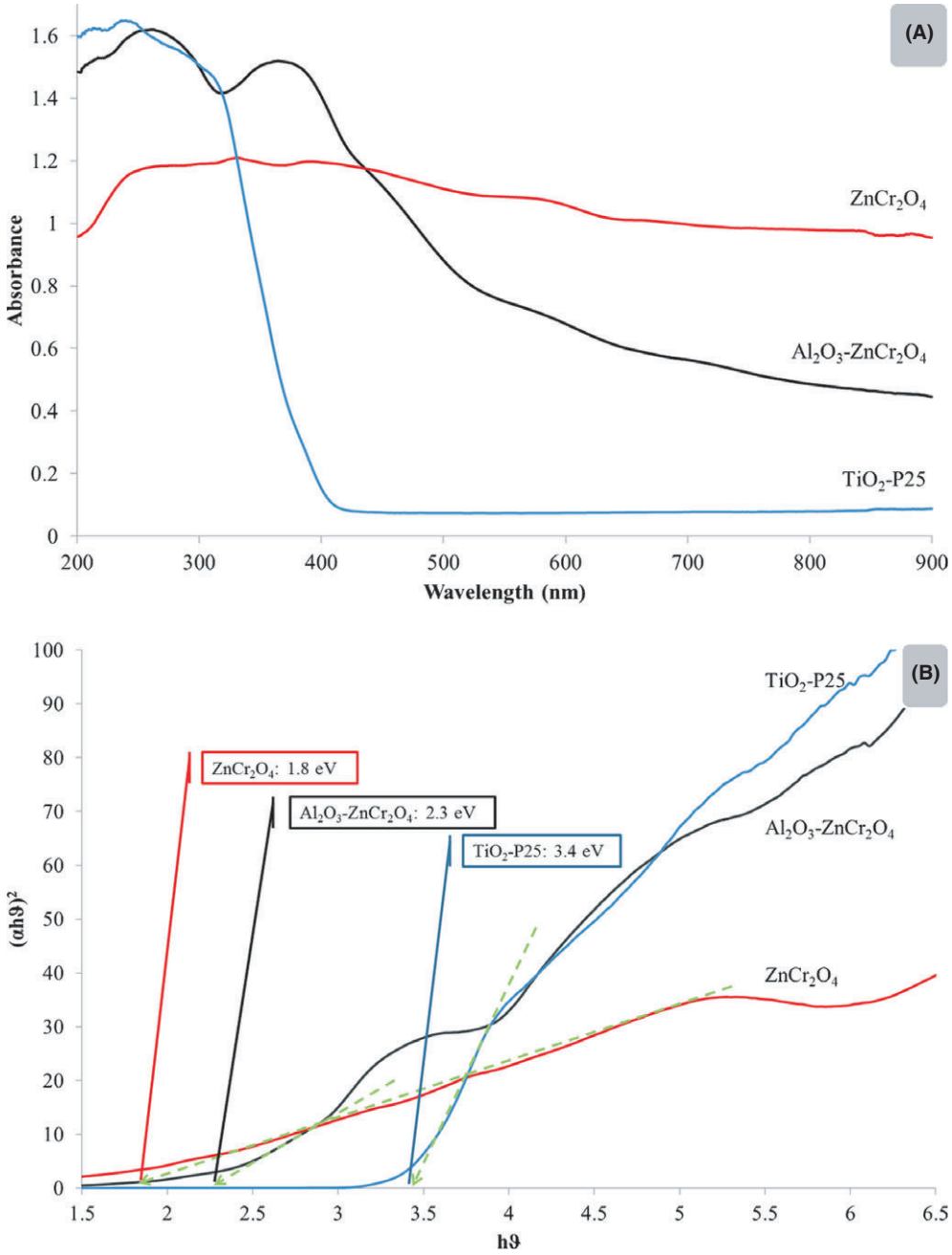

FIGURE 6 (A) The optical absorption spectra (UV-DRS) of the as-synthesized Al_2O_3- $ZnCr_2O_4$, $ZnCr_2O_4$, and TiO_2-P25 powders. (B) Estimation of the E_g values based on the Tauc method. [Color figure can be viewed at wileyonlinelibrary.com]

photocatalyst particles. It has been approved that the photoactivity is improving in respect to the surface area of photocatalyst particles.[35] This means that the recombination rate is more than the surface generation rate. In the case of $ZnCr_2O_4$ NPs, the recombination rate would be slower than that of Al_2O_3- $ZnCr_2O_4$, demonstrating the short lifetime of photogenerated carriers of $ZnCr_2O_4$ NPs and was remarkably enhanced after the formation of the mentioned NPs on the surface of Al_2O_3 particles. Therefore, it can be concluded that the stability of photogenerated electron-hole pairs in Al_2O_3- $ZnCr_2O_4$ sample are as long as required to expedite a reaction on the surface. This phenomenon may be refers to the photocatalytic activity could be correlated with the relationship between the specific surface area and the surface reaction rate.

Multiple promotion influences on the absorbance (see Figure 6A) and photoactivity (see Figure 7) of $ZnCr_2O_4$ NPs by deposition on Al_2O_3 particles can be observed. The photocatalytic activity was reported to be proportional to the degree of crystallinity,[32,36] particle size,[32]

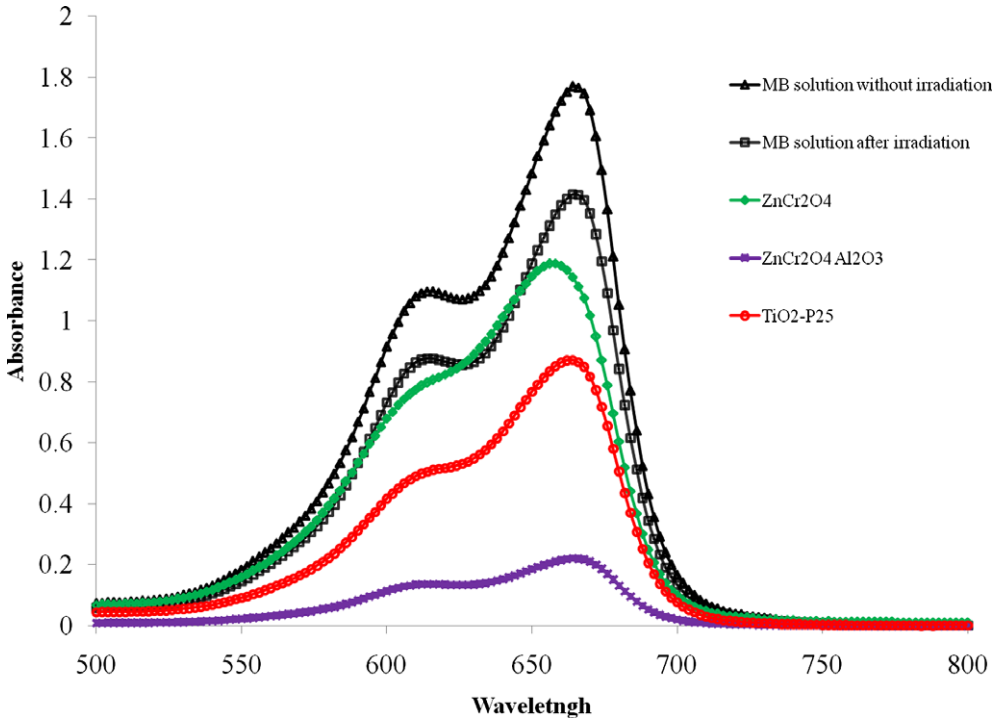

FIGURE 7 UV-visible absorption spectra of the photo-degradation of MB solutions due to the as-synthesized Al_2O_3- $ZnCr_2O_4$ and $ZnCr_2O_4$ powders along with TiO_2-P25 photoactivated after 2 h UV irradiation. [Color figure can be viewed at wileyonlinelibrary.com]

and specific surface area.[32,37] This assertion may be mentioned in terms of the higher degree of crystallinity, smaller crystallite size, and larger surface area. The first one is a significant parameter to analyses the photo-induced behaviors of semiconductors. It has been reported that this behavior enhances with increase in the degree of crystallinity.[38] The smaller crystallite size the more specific surface area, providing more active sites to exhibit more effective photoactivity. On the other hand, size of the crystallites affects the semiconductor band gap, recombination rate, and redox ability. The smaller crystallite size the more powerful redox ability. It is due to this fact that decrease in crystallite size may induce increase in band gap energy, reducing electron-hole recombination rate.[39] Therefore, any agent can lead to change the parameters such as crystallinity, specific surface area, and crystallite size, incurring the characteristics such as photocatalytic activity and absorbance.

The mentioned process in this manuscript leads to form $ZnCr_2O_4$ NPs on the surface of Al_2O_3 particles, preventing the agglomeration, increasing the specific surface area, decreasing the pore size, and increasing the pore volume. As the absorption is a surface area phenomenon, the higher absorption intensity of the as-synthesized composite powder is related to the existence of Al_2O_3 particles. This is because of the influence of Al_2O_3 particles which will influence how $ZnCr_2O_4$ NPs are precipitated and formed with smaller crystallite size and higher specific surface area (see Table 1 and Figures 2,5).

The characteristics of the as-synthesized composite powder make it a remarkable candidate for the applications that require high chemical and thermal stability, high adsorbility and enhanced photocatalytic activity, porous structure and high volume to mass ratio.

4 | CONCLUSION

The Al_2O_3- $ZnCr_2O_4$ nanocomposite powder was synthesized in situ by a heterogeneous precipitation technique using zinc acetate dehydrate, chromium nitrate, aluminum hydroxide powder, and urea precipitation agent. With regard to other methods, the motivation of the mentioned technique is to decrease the agglomeration process (which is inevitable during NPs preparation), to increase the specific surface area and therefore to facilitate the photocatalytic reaction in the active sites of $ZnCr_2O_4$ particles on the surfaces of alumina micron-sized particles. The obtained results clearly validate the performance of the proposed method for increasing the surface area and pore volume and therefore improving the photoactivity of the as-synthesized Al_2O_3- $ZnCr_2O_4$ nanocomposite in comparison with the $ZnCr_2O_4$ NPs. As the Al_2O_3 particles and $ZnCr_2O_4$ NPs were formed simultaneously, the Al_2O_3 particles act as

the crystallization sites of the $ZnCr_2O_4$ NPs, preventing the agglomeration. This process leads to enhance the UV absorbance, photocatalytic behavior and dye removal efficiency with respect to pristine $ZnCr_2O_4$ NPs. However, the dye removal efficiency reached to 86% after 2 h of UV irradiation which is higher than that of the commercial TiO_2-P25 NPs and the pure $ZnCr_2O_4$ NPs. Therefore, a novel photocatalyst composite powder has been prepared with low cost and high performance for the dye removal process.

REFERENCES

1. Sickafus KE, Wills JM, Grimes NW. Structure of spinel. *J Am Ceram Soc*. 1999;82:3279–3292.
2. Ganesh I. A review on magnesium aluminate ($MgAl_2O_4$) spinel: synthesis, processing and applications. *Int Mater Rev*. 2013;58:63–112.
3. Li X, Zhu Z, Zhao Q, Wang L. Photocatalytic degradation of gaseous toluene over $ZnAl_2O_4$ prepared by different methods: a comparative study. *J Hazard Mater*. 2011;186:2089–2096.
4. Galetti AE, Gomez MF, Arrúa LA, Abello MC. Ni catalysts supported on modified $ZnAl_2O_4$ for ethanol steam reforming. *Appl Catal A*. 2010;380:40–47.
5. Zawadzki M, Staszak W, López-Suárez FE, Illán-Gómez MJ, Bueno-López A. Preparation, characterisation and catalytic performance for soot oxidation of copper-containing $ZnAl_2O_4$ spinels. *Appl Catal A*. 2009;371:92–98.
6. Illés E, Szekeres M, Kupcsik E, et al. PEGylation of surfacted magnetite core–shell nanoparticles for biomedical application. *Colloids Surf A*. 2014;460:429–440.
7. Cheraghipour E, Tamaddon AM, Javadpour S, Bruce IJ. PEG conjugated citrate-capped magnetite nanoparticles for biomedical applications. *J Magn Magn Mater*. 2013;328:91–95.
8. Madrakian T, Afkhami A, Ahmadi M. Simple in situ functionalizing magnetite nanoparticles by reactive blue-19 and their application to the effective removal of Pb2+ ions from water samples. *Chemosphere*. 2013;90:542–547.
9. Tang SCN, Lo IMC. Magnetic nanoparticles: essential factors for sustainable environmental applications. *Water Res*. 2013;47:2613–2632.
10. Bakhshayesh S, Dehghani H. Synthesis of magnetite-porphyrin nanocomposite and its application as a novel magnetic adsorbent for removing heavy cations. *Mater Res Bull*. 2013;48:2614–2624.
11. Pokhrel S, Jeyaraj B, Nagaraja KS. Humidity-sensing properties of $ZnCr_2O_4$–ZnO composites. *Mater Lett*. 2003;57:3543–3548.
12. Peng C, Gao L. Optical and photocatalytic properties of spinel $ZnCr_2O_4$ nanoparticles synthesized by a hydrothermal route. *J Am Ceram Soc*. 2008;91:2388–2390.
13. Kagomiya I, Sawa H, Siratori K, et al. Structural phase transition and dielectric properties of $ZnCr_2O_4$. *Ferroelectrics*. 2002;268:327–332.
14. Szymczak H, Wardzyński W, Pajczkowska A. Optical spectrum of antiferromagnetic spinels $ZnCr_2O_4$. *J Magn Magn Mater*. 1980;15–18(Part 2):841–842.
15. Marinković Stanojević ZV, Romčević N, Stojanović B. Spectroscopic study of spinel $ZnCr_2O_4$ obtained from mechanically activated ZnO–Cr_2O_3 mixtures. *J Eur Ceram Soc*. 2007;27:903–907.
16. Gabr RM, Girgis MM, El-Awad AM, Abou-Zeid BM. Effect of spinel ($ZnCr_2O_4$) formation on the texture, electrical conduction and catalytic behaviour of the ZnO–Cr_2O_3 system. *Mater Chem Phys*. 1994; 39:53–62.
17. Yazdanbakhsh M, Khosravi I, Goharshadi EK, Youssefi A. Fabrication of nanospinel $ZnCr_2O_4$ using sol–gel method and its application on removal of azo dye from aqueous solution. *J Hazard Mater*. 2010;184:684–689.
18. Liang Y-C, Cheng Y-R, Hsia H-Y, Chung C-C. Fabrication and reducing gas detection characterization of highly-crystalline p-type zinc chromite oxide thin film. *Appl Surf Sci*. 2016;364:837–842.
19. Hosseini SA, Alvarez-Galvan MC. Study of physical–chemical properties and catalytic activities of $ZnCr_2O_4$ spinel nano oxides obtained from different methods—modeling the synthesis process by response surface methodology and optimization by genetic algorithm. *J Taiwan Inst Chem Eng*. 2016;61:261–269.
20. Liu N, Yuan Z, Wang C, Wang S, Zhang C, Wang S. The role of CeO_2–ZrO_2 as support in the ZnO–$ZnCr_2O_4$ catalysts for autothermal reforming of methanol. *Fuel Process Technol*. 2008;89:574–581.
21. Liu N, Yuan Z, Wang S, Zhang C, Wang S, Li D. Characterization and performance of a ZnO–$ZnCr_2O_4$/CeO_2–ZrO_2 monolithic catalyst for methanol auto-thermal reforming process. *Int J Hydrogen Energy*. 2008;33:1643–1651.
22. Gingasu D, Mindru I, Patron L, et al. Precursor method—a nonconventional route for the synthesis of $ZnCr_2O_4$ spinel. *J Phys Chem Solids*. 2013;74:1295–1302.
23. Mousavi Z, Soofivand F, Esmaeili-Zare M, Salavati-Niasari M, Bagheri S. $ZnCr_2O_4$ nanoparticles: facile synthesis, characterization, and photocatalytic properties. *Sci Rep*. 2016;6:20071.
24. Tajizadegan H, Heidary A, Torabi O, Golabgir M-H, Jamshidi A. Synthesis and characterization of $ZnCr_2O_4$ nanospinel prepared via homogeneous precipitation using urea hydrolysis. *Int J Appl Ceram Technol*. 2016;13:289–294.
25. Tajizadegan H, Jafari M, Rashidzadeh M, Saffar-Teluri A. A high activity adsorbent of ZnO–Al_2O_3 nanocomposite particles: synthesis, characterization and dye removal efficiency. *Appl Surf Sci*. 2013;276: 317–322.
26. Tajizadegan H, Torabi O, Heidary A, Golabgir M-H, Siampour F. Influence of different alumina precursors on structural properties and morphology of ZnO-Al_2O_3 nanocomposite powder. *Int J Appl Ceram Technol*. 2015;12:E162–E169.
27. Daněk O, Štengl V, Bakardjieva S, Murafa N, Kalendová A, Opluštil F. Nanodispersive mixed oxides for destruction of warfare agents prepared by homogeneous hydrolysis with urea. *J Phys Chem Solids*. 2007;68:707–711.
28. Vogels RJMJ, Kloprogge JT, Geus JW. Homogeneous forced hydrolysis of aluminum through the thermal decomposition of urea. *J Colloid Interface Sci*. 2005;285:86–93.
29. Udert KM, Larsen TA, Biebow M, Gujer W. Urea hydrolysis and precipitation dynamics in a urine-collecting system. *Water Res*. 2003;37:2571–2582.
30. Shen X-Q, Jing M-X, Li W-X, Li D-H. Fabrication of Fe-, Ni- and FeNi-coated Al_2O_3 core-shell microspheres by heterogeneous precipitation. *Powder Technol*. 2005;160:229–233.
31. Viezbicke BD, Patel S, Davis BE, Birnie DP. Evaluation of the Tauc method for optical absorption edge determination: ZnO thin films as a model system. *Phys Status Solidi B*. 2015;252:1700–1710.
32. Kim DS, Kwak S-Y. The hydrothermal synthesis of mesoporous TiO_2 with high crystallinity, thermal stability, large surface area, and enhanced photocatalytic activity. *Appl Catal A*. 2007;323:110–118.
33. Lei H-W, Zhang H, Wang X-M, et al. Measurement of ZnO/Al_2O_3 heterojunction band offsets by in situ X-ray photoelectron spectroscopy. *Chin Phys Lett*. 2013;30:118201.
34. Serin T, Serin N, Karadeniz S, Sarı H, Tuğluoğlu N, Pakma O. Electrical, structural and optical properties of SnO_2 thin films prepared by spray pyrolysis. *J Non-Cryst Solids*. 2006;352:209–215.
35. Mazinani B, Masrom AK, Beitollahi A, Luque R. Photocatalytic activity, surface area and phase modification of mesoporous SiO_2–TiO_2 prepared by a one-step hydrothermal procedure. *Ceram Int*. 2014;40(Part A):11525–11532.

36. Naghibi S, Faghihi Sani MA, Madaah Hosseini HR. Application of the statistical Taguchi method to optimize TiO_2 nanoparticles synthesis by the hydrothermal assisted sol–gel technique. *Ceram Int*. 2014;40:4193–4201.
37. Amano F, Nogami K, Tanaka M, Ohtani B. Correlation between surface area and photocatalytic activity for acetaldehyde decomposition over bismuth tungstate particles with a hierarchical structure. *Langmuir*. 2010;26:7174–7180.
38. Peng T, Zhao D, Dai K, Shi W, Hirao K. Synthesis of titanium dioxide nanoparticles with mesoporous anatase wall and high photocatalytic activity. *J Phys Chem B*. 2005;109:4947–4952.
39. Yu JC, Zhang L, Yu J. Direct sonochemical preparation and characterization of highly active mesoporous TiO_2 with a bicrystalline framework. *Chem Mater*. 2002;14:4647–4653.

How to cite this article: Tajizadegan, H., Naghibi, S., Jamshidi, A., Torabi, O. and Golabgir, M.-H. (2016), In situ synthesis of Al_2O_3-supported $ZnCr_2O_4$ nanoparticles for application as an activated photocatalyst. International Journal of Applied Ceramic Technology, 00: 000–000. doi: 10.1111/ijac.12623.